tion. The shoulder at ~0.8μm is due to the instrument throughput.

To show the up-conversion, we used a semiconductor laser diode with an InGaAsP active region designed for 1.6μm emission at room temperature. The emission spectrum is shown in Fig. 3. The 1.6μm laser emission was used to excite the *pin* photodiode. The LED emission induced by the resulting photocurrent was detected by an Si photodiode. The emission spectrum is shown in Fig. 3, corresponding to the $InAs_{0.1}P_{0.9}$ bandgap (1μm). The concept of up-conversion is thus clearly demonstrated.

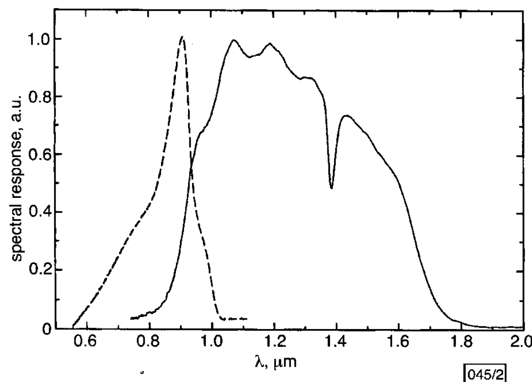

Fig. 2 *Room temperature spectral photoresponse curves*

——— photodiode response
– – – – response of LED structure under reverse bias

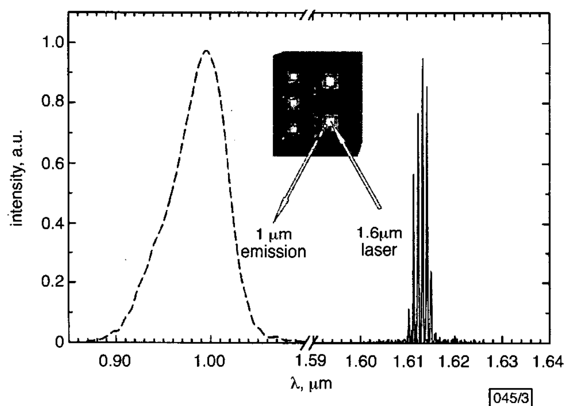

Fig. 3 *Room temperature emission spectra*

Diode laser is used to excite the photodiode
——— diode laser emission spectrum
– – – – LED emission spectrum
Inset: measurement geometry

To produce a useful device, the efficiencies for both the PD and LED must be high. The efficiency of our *pin* photodiode is not an issue. In a separate calibration measurement using a similar PD, we measured a responsivity value of ~2A/W, implying a high absorption efficiency (≃ 100%). The efficiency of our present LED is low. We estimate a value of < 1% internal quantum efficiency. One of the main factors is the poor carrier confinement due to the small bandgap difference between $InAs_{0.1}P_{0.9}$ and InP. At room temperature, carriers easily escape the active region. Indeed, when the temperature is reduced to ~77K, the LED efficiency increases by a factor of ~300. This demonstrates that the material quality is high and that the main problem is the poor carrier confinement. To improve the LED efficiency, we need to increase the bandgap difference between the active region and the carrier confining regions. The As fraction in the active region could be increased, but the strain will be higher. For a 60nm thickness, the coherent strain critical As alloy value is ~20%. Furthermore, a higher As fraction will shift the emission wavelength to a longer value. Beyond a wavelength of ~1μm, the CCD response degrades rapidly. Another approach is to use InP or low As fraction InAsP as the LED active region and InGaP (with low Ga fraction) in the confining regions.

There are other areas that need further study. (i) The downward emitted light which reaches the detector active region should be absorbed, which leads to a 'recycling' and positive feedback effect. This effect may leads to an improvement of the LED external efficiency. (ii) The detector does not need to be a photodiode. A photoconductor may be used, which may result in a more stable circuit configuration than the present back-to-back diode configuration. (iii) Through appropriate design, the excitation-detection-emission process could have little lateral spreading. This enables the fabrication of a pixelless imaging device. One of the key factors is to make sure that the middle contact layer is thin and completely depleted under operating bias.

In conclusion, we have demonstrated an up-conversion device for wavelengths from 1.2–1.6 to 1μm. The immediate intended application involves detecting a scene illuminated by a 1.5μm laser, eye-safe in comparison with existing systems using lasers in 800–900nm wavelengths [7]. The eventual device acts as an image converter with the output captured by a conventional CCD or image intensifying camera. Further studies are underway to improve the LED efficiency and to shift the output wavelength to a higher energy.

Acknowledgments: The authors thank S. Rolfe for the SIMS measurements, and P. Marshall for the device fabrication. They also thank E. Dupont, B.J. Robinson, and D.A. Thompson for fruitful discussions. The work was supported in part by DREV of the Department of National Defence.

© Canadian Crown Copyright 2000
18 May 2000
Electronics Letters Online No: 20000915
DOI: 10.1049/el:20000915

H.C. Liu, M. Gao and P.J. Poole (*Institute for Microstructural Sciences, National Research Council, Ottawa, Ontario K1A 0R6, Canada*)

References

1 KRUSE, P.W., PRIBBLE, F.C., and SCHULZE, R.G.: 'Solid-state infrared-wavelength converter employing high-quantum-efficiency Ge-GaAs heterojunction', *J. Appl. Phys.*, 1967, **38**, pp. 1718–1720

2 LIU, H.C., LI, J., WASILEWSKI, Z.R., and BUCHANAN, M.: 'Integrated quantum well intersubband photodetector and light emitting diode', *Electron. Lett.*, 1995, **31**, pp. 832–833

3 LIU, H.C., ALLARD, L.B., BUCHANAN, M., and WASILEWSKI, Z.R.: 'Pixelless infrared imaging device', *Electron. Lett.*, 1997, **33**, pp. 379–380

4 DUPONT, E., LIU, H.C., BUCHANAN, M., WASILEWSKI, Z.R., ST-GERMAIN, D., and CHEVRETTE, P.: 'Pixel-less infrared imaging based on the integration of an n-type quantum-well infrared photodetector with a light-emitting diode', *Appl. Phys. Lett.*, 1999, **75**, pp. 563-565

5 GURNEY, M.L., and KELLY, J.: 'The design and field testing of a 1.5μm active TV system', *SPIE*, 1999, **3698**, pp. 244–249

6 OLSEN, G.H., LANGE, M.J., SUGG, A.R., ETTENBERG, M.H., SUDOL, J.J., and FORREST, S.R.: 'Characterization of InP substrates for large-area focal plane arrays', *Compound Semicond.*, 1999, **8**, pp. 62–66

7 MILLER, J.L., and LITTLE, D.: 'Catching polluters (infra)red-handed', *Photonics Spectra*, 2000, **34**, pp. 144–145

High detectivity InGaAsSb *pin* infrared photodetector for blood glucose sensing

B.L. Carter, E. Shaw, J.T. Olesberg, W.K. Chan, T.C. Hasenberg and M.E. Flatté

A molecular beam epitaxy grown GaInAsSb *pin* photodetector lattice matched to a GaSb substrate is reported. The mesa type detector has high responsivity in the 1.4 to 2.4μm wavelength range with –0.3V bias, 40μA dark current for a 1mm diameter detector and the highest detectivity D^* of $2.6 \times 10^{10} cm \cdot Hz^{1/2}/W$ reported for a GaInAsSb detector. The measured responsivity compares well with $k \cdot p$ calculations.

Many biological molecules and atmospheric pollutants have distinctive absorption lines in the near and mid-infrared part of the spectrum, making this an important spectral range for chemical sensing. For example, an application of interest to us is the non-invasive, *in vivo*, monitoring of glucose levels in the blood. The optical absorption spectrum from 2–2.4μm, where human tissue is highly scattering though relatively lossless, is correlated with the blood glucose level so that a continuous measurement of the absorption spectrum gives a continuous measure of the glucose level in a patient. The signal for this and other sensing applications is often very weak, so it is critical that the noise at the detector be low. The signal for glucose monitoring can be increased with a 1–2mm diameter detector that collects most of the scattered light. Despite the reduction in detector speed due to the increase in capacitance with the detector area A, the speed is still adequate for our application. Detector noise in the absence of a strong signal is dominated by fluctuations in the dark current and in the photocurrent originating from background radiation [1], which are proportional to $\sqrt{A}$. Thus, the detector should be just large enough to collect the signal, be responsive only in the wavelength range of interest and have low dark current to maximise the signal-to-noise ratio.

The wavelengths for blood glucose monitoring are beyond the absorption edge at a bandgap wavelength λ_g = 1.7μm in the $In_{0.53}Ga_{0.47}As$-InP material system, where *pin* photodetectors are well developed for optical communications. Although the absorption can be extended to longer wavelengths with a lattice mismatched $In_{0.53+\delta}Ga_{0.47-\delta}As$ absorption layer, the thickness of this layer is well beyond the critical thickness in a typical detector and the resulting misfit dislocations are potentially a source of generation currents and carrier traps which will add to the detector noise. The GaSb system is a promising candidate for detectors in the $\lambda_g \geq$ 1.7μm wavelength range because many lattice matched and strain compensated alloys with appropriate bandgap energies can be formed [2 – 8].

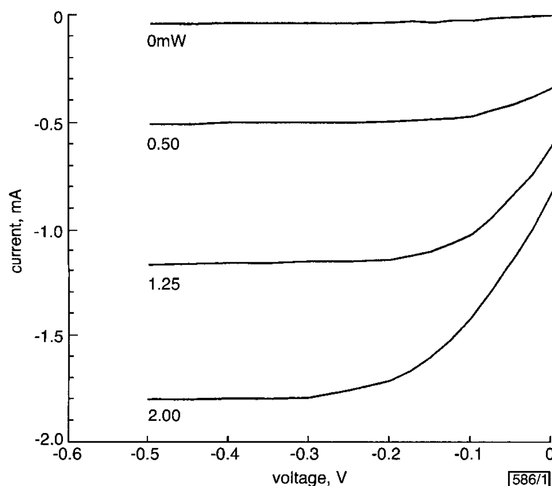

Fig. 1 *Room temperature reverse biased I-V characteristics of 1mm diameter detector under various incident powers at 1.55μm*

We report here *pin* photodetectors that are responsive to 2.4μm light and lattice matched to GaSb. The device, grown by molecular beam epitaxy on a p-GaSb substrate, consists of a 400nm p-GaSb buffer layer, a 500nm p-$In_{0.19}Ga_{0.81}As_{0.17}Sb_{0.83}$ (λ_g = 2.38μm) p-clad, a 1.5μm unintentionally doped i-$In_{0.19}Ga_{0.81}As_{0.17}Sb_{0.83}$ (λ_g = 2.38μm) absorption layer, a 1.5μm strain compensated superlattice n-clad (λ_g = 1.25μm) formed by alternating 1.1nm InAs and 2.7nm $Al_{0.60}Ga_{0.40}Sb$ layers, and a 10nm n-InAs contact layer. Although the n-clad could be grown with a smaller bandgap by altering the superlattice composition, the larger bandgap clad allowed us to test the photodetectors with a 1.55μm laser. X-ray diffraction verified that the epitaxial layers are well lattice matched to the GaSb substrate.

Photodetectors were fabricated by first patterning ring or wagon wheel shaped n-type ohmic contacts of 15nm Ti/200nm Au by lift-off. The metal was deposited onto the n-InAs layer by electron beam evaporation. Mesas were then etched to the p-clad using citric acid, phosphoric acid, hydrogen peroxide and water with a photoresist mask. To complete the fabrication, 15nm Ti/200nm Au were evaporated completely over the back to form the p-type ohmic contact. The contacts were not alloyed. The photodetectors were not antireflection coated.

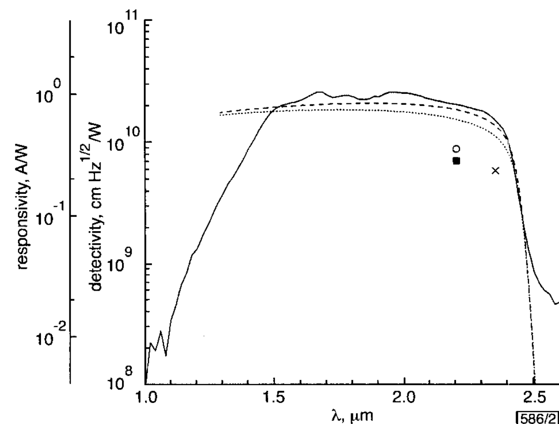

Fig. 2 *Room temperature detectivity of 1mm diameter detector illuminated by blackbody source and biased at –0.3V, calculated values of detectivity for two different cases, and previously reported detectors*

——— room temperature detectivity
·········· calculated detectivity, no diffusion from p-clad
– – – – calculated detectivity, diffusion length much greater than p-clad thickness
■ Srivastava *et al.* [3]
○ Tournié *et al.* [5]
× Shi *et al.* [7]
Auxiliary scale applies to this detector only

The room temperature I-V characteristics of a 1mm diameter photodetector under various intensity illumination from a 1.55μm laser is shown in Fig. 1. The flatness of the I-V characteristics beyond –0.3V of bias indicates that most of the photogenerated carriers are collected from the depletion region. The dark current is ~40μA at –0.3V. The responsivity R at this wavelength is 0.88A/W, corresponding to a 70% external quantum efficiency. The 30% loss is accountable by surface reflections of the uncoated detectors. The response of the same detector to longer wavelengths (Fig. 2) was determined with a 1000°C blackbody source scanned at 2.0nm resolution and normalised with the responsivity at 1.55μm. The detectivity D^* was obtained with the measured dark current as the noise source. Peaks in the spectrum are due to atmospheric absorption. D^* has a maximum value of 2.6 × 10^{10}cm·Hz$^{1/2}$/W, with a corresponding R of 1.04A/W, and it remains high until near the bandedge of the absorption layer at $\lambda \simeq$ 2.4μm. Reported high detectivities at room temperature [3, 5, 7] are between 5.8 – 8.8 × 10^9cm·Hz$^{1/2}$/W and are indicated in Fig. 2.

As mentioned above, light outside the spectral range where we expect useful information adds to the noise and contributes nothing to the signal. While the short wavelength cutoff of the detector can be adjusted by the bandgap energy of the clad on the incident side of the junction with little effect on other aspects of photodetector performance, the long wavelength cutoff is determined by the bandgap of the absorption layer. The absorption coefficient α of this layer is closely coupled to the responsivity, speed and noise performance of the photodetector, so it is important to know $\alpha(\lambda)$ accurately. This is particularly important for photodetectors operating near the bandedge where α depends strongly on wavelength. Fig. 2 shows the detectivity derived from the observed dark current and from $\alpha(\lambda)$ calculated using an eight band $k{\cdot}p$ model. The calculated absorption spectrum was convoluted with a Gaussian distribution of bandgap energies with a half-width of 4meV to improve the fit near the bandedge. Such a distribution can arise from variations in the composition of the absorption layer. Absorption by the n-clad, which is responsible for the short wavelength cutoff, was not included in the calculation.

Although the agreement is reasonably good, the measurements are systematically higher than the calculations. The difference may be due to carriers photogenerated within a diffusion length of the depletion region. These carriers contribute to the photocurrent

even though the electrons and holes are not separated by the electric field. If the diffusion length is greater than the p-clad thickness, the effective absorption layer thickness for wavelengths longer than the bandgap wavelength of GaSb (1.71 μm) is the sum of the i-layer and p-clad thicknesses. At shorter wavelengths, the effective absorption layer thickness can be even greater because photogeneration occurs in the GaSb buffer and substrate. The calculation with an effective thickness of 2.0μm shows much better agreement with the measurements. Diffusion of carriers is often undesirable because it gives a slow tail in the detector impulse response. The tail for minority electrons diffusing 1μm is < 1ns, much faster than the microsecond to millisecond response required for chemical sensors.

In summary, we have made InGaAsSb *pin* photodetectors lattice matched to GaSb with a high responsivity for wavelengths of interest for chemical sensing. The absorption coefficient near the bandgap agrees well with our calculations. Although the dark current is 40μA for a 1mm diameter detector, we believe even lower dark currents can be achieved with a diffused rather than a mesa structure.

Acknowledgment: We gratefully acknowledge the support of the National Institutes of Health.

© IEE 2000
7 June 2000
Electronics Letters Online No: 20000956
DOI: 10.1049/el:20000956

B.L. Carter and W.K. Chan (*Department of Electrical and Computer Engineering, Optical Science and Technology Center, University of Iowa, Iowa City, IA 52242, USA*)

E. Shaw, J.T. Olesberg, T.C. Hasenberg and M.E. Flatté (*Department of Physics and Astronomy, Optical Science and Technology Center, University of Iowa, Iowa City, IA 52242, USA*)

References

1 KINGSTON, R.H.: 'Detection of optical and infrared radiation' (Springer-Verlag, Berlin, 1978), p. 69
2 ANDREEV, I.A., AFRAILOV, M.A., BARANOV, A.N., DANIL'CHENKO, V.G., MIRSAGATOV, M.A., MIKHAILOVA, M.P., and YAKOVLEV, YU.P.: 'GaInAsSb/GaAlAsSb solid-solution photodiodes', *Sov. Tech. Phys. Lett.*, 1986, **12**, pp. 542–544
3 SRIVASTAVA, A.K., DEWINTER, J.C., CANEAU, C., POLLACK, M.A., and ZYSKIND, J.L.: 'High performance GaInAsSb-GaSb p-n photodiodes for the 1.8–2.3μm wavelength region', *Appl. Phys. Lett.*, 1986, **48**, pp. 903–904
4 MEBARKI, M., BELATOUI, T., JOULLIÉ, A., ORSAL, B., and ALABEDRA, R.: 'Reverse current and external quantum efficiency of zinc diffused 1.3μm GaAlAsSb photodiode', *J. Appl. Phys.*, 1990, **63**, pp. 4106–4110
5 TOURNIÉ, E., LAZZARI, J.-L., VILLEMAIN, E., JOULLIÉ, A., GOUSKOV, L., KARIM, M., and SALESSE, I.: 'GaInAsSb/GaSb *pn* photodiodes for detection to 2.4μm', *Electron. Lett.*, 1991, **27**, pp. 1237–1239
6 ZHANG, B., ZHOU, T., JIANG, H., NING, Y., and JIN, Y.: 'GaInAsSb/GaSb infrared photodetectors prepared by MOCVD', *Electron. Lett.*, 1995, **31**, pp. 830–832
7 SHI, Y., ZHAO, J.H., LEE, H., SARATHY, J., COHEN, M., and OLSEN, G.: 'Resonant cavity enhanced GaInAsSb photodetectors grown by MBE for room temperature operation at 2.35μm', *Electron. Lett.*, 1996, **32**, pp. 2268–2269
8 CHOI, H.K., WANG, C.A., TURNER, G.W., MANFRA, M.J., SPEARS, D.L., CHARACHE, G.W., DANIELSON, L.R., and DEPOY, D.M.: 'High-performance GaInAsSb thermophotovoltaic devices with an AlGaAsSb window', *Appl. Phys. Lett.*, 1997, **71**, pp. 3758–3760

InP-based 1300nm microcavity LEDs with 9% quantum efficiency

B. Depreter, I. Moerman, R. Baets, P. Van Daele and P. Demeester

InP-based microcavity light emitting diodes (MCLEDs) operating at a wavelength of 1300nm are reported. An output power of 3.8mW and total external quantum efficiency of 9% are reported. These values are to the best of the authors' knowledge the highest ever reported for an InP-based MCLED.

Introduction: In the GaAs material system, the microcavity concept has proven to be very successful in increasing the overall quantum efficiency of light emitting diodes (LEDs) [1, 2].

In the InP material system, the reduced refractive index contrast generates substantial difficulties when creating a good distributed Bragg reflector (DBR). This problem is well known for long wavelength vertical cavity surface emitting lasers (VCSELs), although for a different reason. VCSELs need highly reflective mirrors, and thus a very high number of mirror pairs in their DBRs. Since MCLEDs are spontaneous emission devices, there is no need for such a high number of mirror pairs; to improve the output characteristics of the LED it is even necessary that the outcoupling mirror has a relatively low reflectivity. The main problem with the low refractive index contrast is that it enlarges the penetration depth into the DBR. This increases the cavity length, and the number of modes supported by the cavity m_c. The maximum extraction efficiency of a microcavity LED is inversely proportional to m_c [3].

In this Letter we demonstrate the successful fabrication of InP-based microcavity light emitting diodes, obtaining high output power and high total external quantum efficiency.

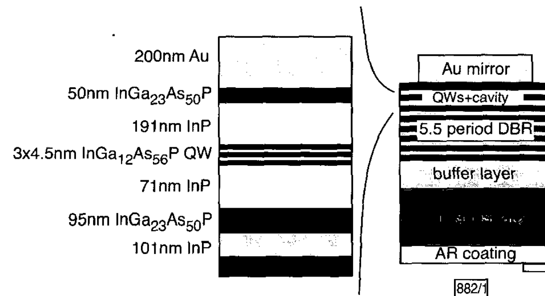

Fig. 1 *Structure of MCLED*

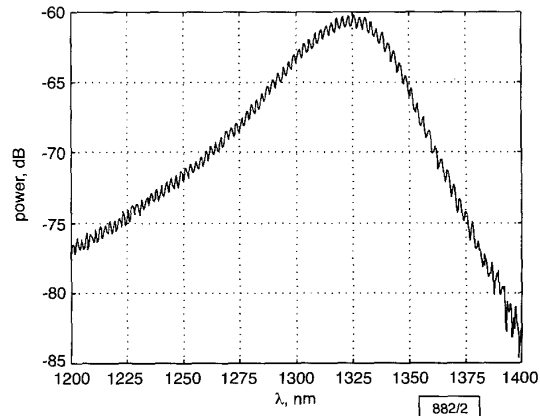

Fig. 2 *Spectrum of 215μm diameter MCLED*

Device fabrication: All layers were grown by means of metal-organic vapour phase epitaxy in a 3×2" Thomas Swan vertical reactor. The precursors were TMI, TMG, TMA, pure PH_3 and pure AsH_3. H_2S was used as an n-dopant, DEZ for p-doping. The substrate was a 2-inch ⟨100⟩ exact oriented n-type wafer. All device layers were grown at a pressure of 76Torr and at a temperature of 630°C.

InP MCLEDs with a structure as presented in Fig. 1 were fabricated. The active region emitting at 1320nm consisted of three compressively strained $InGa_{0.12}As_{0.56}P$ quantum wells (4.5nm) embedded within 10nm $InGa_{0.145}As_{0.317}P$ barriers. The bottom DBR consists of 5.5 periods of alternating 101nm InP and 95nm $InGa_{0.23}As_{0.50}P$.

The wafer was processed as follows. On top of the devices 200nm of Au was deposited to serve both as the highly reflective top mirror and as the p-type contact. Contact diameters of 25, 40, 70, 115, 215, 520, 1030 and 2030μm were realised. Mesas were defined by a shallow self-aligned wet etch, using the metal mirrors as the mask pattern. On the bottom side, the substrate was